



**HAL**  
open science

# Bound states in the continuum in circular clusters of scatterers

Marc Martí-Sabaté, Bahram Djafari-Rouhani, Daniel Torrent

► **To cite this version:**

Marc Martí-Sabaté, Bahram Djafari-Rouhani, Daniel Torrent. Bound states in the continuum in circular clusters of scatterers. *Physical Review Research*, 2023, 5 (1), pp.013131. 10.1103/PhysRevResearch.5.013131 . hal-04079791

**HAL Id: hal-04079791**

**<https://hal.science/hal-04079791>**

Submitted on 25 Apr 2023

**HAL** is a multi-disciplinary open access archive for the deposit and dissemination of scientific research documents, whether they are published or not. The documents may come from teaching and research institutions in France or abroad, or from public or private research centers.

L'archive ouverte pluridisciplinaire **HAL**, est destinée au dépôt et à la diffusion de documents scientifiques de niveau recherche, publiés ou non, émanant des établissements d'enseignement et de recherche français ou étrangers, des laboratoires publics ou privés.




Distributed under a Creative Commons Attribution 4.0 International License

## Bound states in the continuum in circular clusters of scatterers

Marc Martí-Sabaté<sup>1</sup>, Bahram Djafari-Rouhani<sup>2</sup>, and Dani Torrent<sup>1,\*</sup>

<sup>1</sup>*GROC, UJI, Institut de Noves Tecnologies de la Imatge (INIT), Universitat Jaume I, 12071 Castelló de la Plana, Spain*

<sup>2</sup>*IEMN, University of Lille, Cité Scientifique, 59650 Villeneuve d'Ascq, France*

 (Received 10 October 2022; revised 19 January 2023; accepted 1 February 2023; published 21 February 2023)

In this work we study the localization of flexural waves in highly symmetric clusters of scatterers. It is shown that when the scatterers are placed regularly in the perimeter of a circumference, the quality factor of the resonances strongly increases with the number of scatterers in the cluster. It is also found that in the continuous limit, that is to say, when the number of scatterers tends to infinite, the quality factor is infinite so that the modes belong to the class of the so-called bound states in the continuum or BICs, and an analytical expression for the resonant frequency is found. These modes have different multipolar symmetries, and we show that for high multipolar orders the modes tend to localize at the border of the circumference, therefore forming a whispering gallery mode with an extraordinarily high quality factor. Numerical experiments are performed to check the robustness of these modes under different types of disorder and also to study their excitation from the far field. Although we have focused our study on flexural waves, the methodology presented in this work can be applied to other classical waves, like electromagnetic or acoustic waves, being a promising approach for the design of high-quality resonators based on finite clusters of scatterers.

DOI: [10.1103/PhysRevResearch.5.013131](https://doi.org/10.1103/PhysRevResearch.5.013131)

### I. INTRODUCTION

Bound states in the continuum (BICs) are eigenmodes of a system whose energy lies in the radiation part of the spectrum while remaining localized in a finite part of the system and with an infinite lifetime. These states were first mathematically proposed in 1929 by von Neumann and Wigner in the framework of quantum mechanics [1], although the concept has been extended to classical waves, like acoustics [2–6], microwaves [7,8], or optics [9–11].

Despite the fact that the practical realization of BICs is a challenging problem, structures based on them present sharp resonances with extremely high-quality factors, which have as well the advantage, unlike ideal BICs, that they can be excited with external radiative fields. Also named quasi-BICs (or QBICs), these modes have been widely used in sensing applications [12–14]. In recent years, different structures have been studied in order to achieve these high-Q resonances, such as subwavelength gratings [15–18], coupled gratings [12,19], or photonic crystal slabs [20–24], even combined with more complex structures [25].

Among the wide variety of geometries and structures used to find BICs [26], those based on finite structures are specially interesting for practical applications, since periodic or waveguide BICs will always present finite-size effects which

will decrease their efficiency. For instance, circular clusters of scatterers studied in some recent works [14,27] are extraordinarily convenient from a practical point of view. In this work we will generalize the study of these circular clusters of scatterers to provide a general schema for the realization of QBICs based on this geometry.

The manuscript is organized as follows: After this Introduction, in Sec. II we study the formation of bound states in the continuum in open systems by attaching a cluster of mass-spring resonators to a thin elastic plate. We will find that when the scatterers in the cluster are arranged in the corners of a regular polygon, the quality factor of the resonances quickly increases with the number of scatterers in the cluster. In Sec. III we perform several numerical experiments to check the robustness of these modes, and in Sec. IV their excitation from the far field will be considered. Finally, Sec. V summarizes the work.

### II. EIGENMODES OF A POLYGONAL CLUSTER OF SCATTERERS

The propagation of flexural waves in thin elastic plates where a cluster of  $N$  pointlike resonators has been attached at positions  $\mathbf{R}_\alpha$  is described by means of the inhomogeneous Kirchhoff [28] equation,

$$(\nabla^4 - k_0^4)\psi(\mathbf{r}) = \sum_{\alpha=1}^N t_\alpha \delta(\mathbf{r} - \mathbf{R}_\alpha)\psi(\mathbf{r}), \quad (1)$$

where  $\psi(\mathbf{r})$  is the spatial part of the vertical displacement of the plate, which is assumed to be harmonic and of the form

$$W(\mathbf{r}, t) = \psi(\mathbf{r})e^{-i\omega t}. \quad (2)$$

\*dtorrent@uji.es

Published by the American Physical Society under the terms of the [Creative Commons Attribution 4.0 International](https://creativecommons.org/licenses/by/4.0/) license. Further distribution of this work must maintain attribution to the author(s) and the published article's title, journal citation, and DOI.

Also, the free-space wave number  $k_0$  is given by

$$k_0^4 = \frac{\rho h}{D} \omega^2, \quad (3)$$

with  $\rho$ ,  $h$ , and  $D$  being the plate's mass density, height and rigidity, respectively. The response of each resonator is given by the  $t_\alpha$  coefficient, which is a resonant quantity whose properties depend on the geometry of the scatterer attached to the plate [29]. However, for the purposes of the present work, it will be assumed that it can take any real value in the range  $t_\alpha \in (-\infty, \infty)$ .

A self-consistent multiple scattering solution can be found for the above equation as

$$\psi(\mathbf{r}) = \psi_0(\mathbf{r}) + \sum_{\alpha=1}^N B_\alpha G(\mathbf{r} - \mathbf{R}_\alpha), \quad (4)$$

where  $\psi_0(\mathbf{r})$  is the external incident field on the cluster of scatterers,  $G(\mathbf{r})$  is the Green's function of the Kirchhoff equation,

$$G(\mathbf{r}) = \frac{i}{8k_0^2} [H_0(k_0 r) - H_0(ik_0 r)], \quad (5)$$

with  $H_0(\cdot)$  being Hankel's function of first class. The multiple scattering coefficients  $B_\alpha$  can be obtained by means of the self-consistent system of equations

$$\sum_{\beta=1}^N M_{\alpha\beta} B_\beta = \psi(\mathbf{R}_\alpha), \quad (6)$$

where

$$M_{\alpha\beta} = t_\alpha^{-1} \delta_{\alpha\beta} - G(\mathbf{R}_{\alpha\beta}) \quad (7)$$

is the multiple scattering matrix  $M$ .

The eigenmodes of a cluster of  $N$  scatterers attached to a thin elastic plate can be found assuming that there is no incident field, so that the total field excited in the plate is due only to the scattered field by all the particles [30,31]. Under these conditions Eq. (6) becomes a homogeneous system of equations with nontrivial solutions only for those frequencies satisfying

$$\det M(\omega) = 0. \quad (8)$$

For finite clusters of scatterers the above condition can be satisfied only for complex frequencies, being the inverse of the imaginary part of this frequency the quality factor of the resonance. Those configurations in which the imaginary part of the resonant frequency is extraordinarily small (hence the quality factor is extraordinarily big) receive the name of quasi-BIC or QBIC modes. In the following lines it will be shown that by arranging the scatterers in the vertices of regular polygons we can obtain resonances whose quality factor diverges as the number of scatterers approaches infinite.

Then, if the scatterers are all identical with impedance  $t_0$  and they are regularly arranged in a circumference of radius  $R_0$  and placed at angular positions  $2\pi\alpha/N$ , for  $\alpha = 0, \dots, N-1$  (as shown in Fig. 10 in Appendix), the Hamiltonian of the system commutes with the rotation operator  $R_N$ , whose eigenvalues are  $\lambda_\ell = \exp(i2\pi\ell/N)$ , with  $\ell = 0, \dots, N-1$ , and

this implies a relationship between the coefficients of the form [27]

$$B_\alpha^\ell = e^{2i\pi\ell\alpha/N} B_0^\ell, \quad (9)$$

and thus Eq. (6) becomes

$$\left( 1 - t_0 \sum_{\beta=1}^N G(\mathbf{R}_{0\beta}) e^{2i\pi\ell\beta/N} \right) B_0^\ell = 0. \quad (10)$$

It is more suitable now to define the Green's function as

$$G(\mathbf{r}) \equiv ig_0 \xi(\mathbf{r}), \quad (11)$$

where

$$g_0 = \frac{1}{8k_0^2} \quad (12)$$

and

$$\xi(\mathbf{r}) = H_0(k_0 r) - H_0(ik_0 r), \quad (13)$$

so that  $\xi(\mathbf{0}) = 1$  and  $\gamma_0 = t_0 g_0$  is a real quantity. The eigenmodes of the system are found as the nontrivial solutions of Eq. (10), and thus for the  $\ell$ th mode we need to solve

$$1 - i\gamma_0 \sum_{\beta=1}^N \xi(\mathbf{R}_\beta) e^{2i\pi\ell\beta/N} = 0. \quad (14)$$

This equation will give us a set of complex free-space wave numbers  $k_0^n$  from which we can obtain the eigenfrequencies  $\omega_n$  by means of the plate's dispersion relation. The imaginary part of these eigenfrequencies is related with the quality factor of the mode: the lower the imaginary part the larger the quality factor. Consequently, a BIC will be found if we can obtain a real wave number  $k_0^n$  satisfying the above equation. Thus, assuming this wave number exists, we define

$$S^\ell = \sum_{\beta=1}^N \xi_\beta e^{2i\pi\ell\beta/N} = S_R^\ell + iS_I^\ell, \quad (15)$$

and the secular equation can be divided in real and imaginary parts as

$$S_R^\ell(k_0) = 0, \quad (16)$$

$$1 + \gamma_0 S_I^\ell(k_0) = 0. \quad (17)$$

The second of these equations will always be satisfied, since  $\gamma_0$  is a resonant factor that can be selected to run from  $-\infty$  to  $\infty$ . Therefore we have to find the conditions for which the first of the equations can be satisfied.

Figure 1(a) shows the evolution of  $S_R^\ell$  (in logarithmic scale, for clarity) as a function of  $k_0 R_0$  for  $\ell = 0$  and for different numbers of scatterers  $N$  in the cluster. As can be seen, for a small number of scatterers the function does not approach zero, so that no BIC can be found, although for a relatively large number of particles the function is nearly zero, indicating a high-quality resonance. Figure 1(b) shows  $S_R^\ell$  as a function of  $k_0 R_0$  but for a fixed number of scatterers  $N = 10$  and for  $\ell = 0, 1, 2, 3$ . In this case we can see how the function  $S_R^\ell$  is nearly zero for low  $\ell$ , although for  $\ell = 3$  the minimum is actually far away from zero. It is found numerically that these

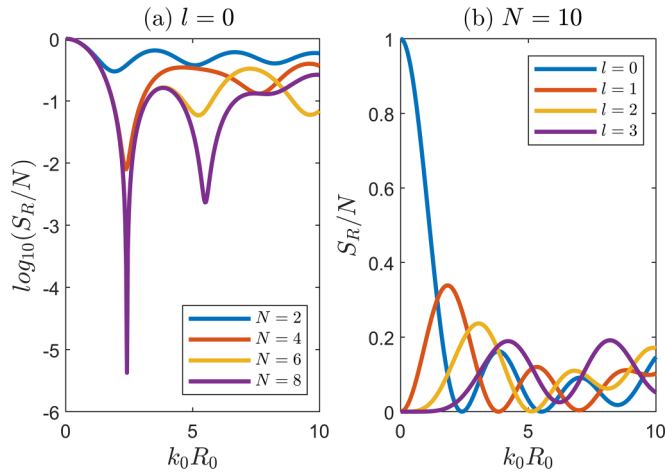


FIG. 1.  $S_R$  summation for different situations. In (a) the different lines correspond to different number of scatterers in the cluster, and the resonance index is fixed at  $l = 0$ . In panel (b), the number of scatterers in the cluster is fixed ( $N = 10$ ) and the evolution of  $S_R/N$  as a function of  $k_0$  is shown for different resonant index.

minima approach zero as we increase the number of scatterers in the cluster, although the zero value is reached only in the limit  $N \rightarrow \infty$ . Indeed, it is found that (see Appendix)

$$\lim_{N \rightarrow \infty} \frac{1}{N} S_R^\ell = J_\ell^2(k_0 R_0), \quad (18)$$

and consequently, the resonances of the cluster are given by the zeros of the Bessel function  $J_\ell(k_0 R_0)$  in this limit, reaching the BIC condition, although in clusters with  $N > 10$  good quality resonances are found, being therefore quasi-BIC modes.

Interestingly, although the position of the resonance should be determined from Eq. (16) and this should depend on  $N$ , in practice we observe that only a few scatterers are enough to make Eq. (18) valid, and for  $N > 10$  we can say that Eq. (18) is the equation determining the resonances of the cluster. The reason for this quick convergence is that above this limit the distance between the scatterers is very small in comparison with the wavelength of the field, and hence all that matters is the ratio between the impedance of the scatterers  $\gamma_0$  [obtained from Eq. (17) and, in general, a function of  $N$ ] and the distance between them, similar to what we find in a homogenization problem. If this ratio is constant the resonant frequency will be the same independently of the number of scatterers. This is the reason as well for which small structural perturbations keep the position of the resonant frequency unchanged, as will be shown later.

However, the imaginary part of the resonant frequency or, equivalently, the quality factor of the resonance changes with both the number of scatterers and structural perturbations. The reason for that is that this is a more sensitive parameter, since in an open cluster we have more channels to lose energy, and any perturbation, like disorder or a reduction of the effective surface impedance, will result in a variation of the quality factor of the resonance.

The quality factor of these resonances can be found by the analysis of the minimum eigenvalue of the multiple

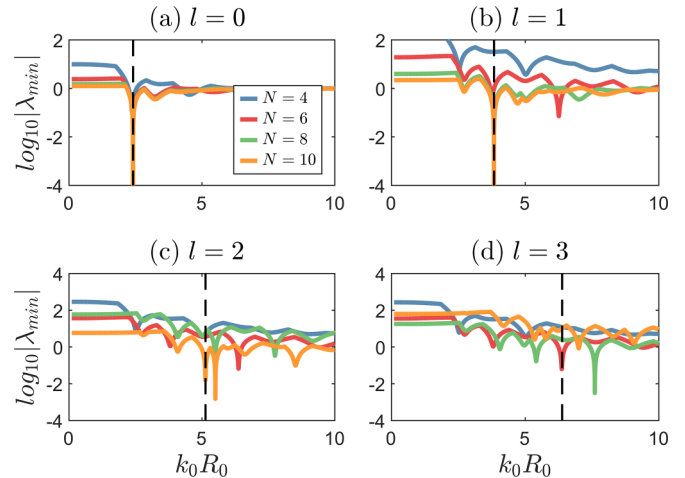


FIG. 2. Resonance comparison for several clusters. Each panel presents the resonances for a different resonant index ( $\ell$ ). The color code is the same for the four panels, representing a different number of scatterers in the cluster (blue is  $N = 4$ , red is  $N = 6$ , green is  $N = 8$ , and orange is  $N = 10$ ). The dashed line indicates the frequency at which the resonance is predicted for an infinite number of scatterers in the cluster.

scattering matrix  $M$ , as was analyzed in detail in Refs. [31,32]. Figures 2(a)–2(d) show this parameter for the modes  $\ell = 0, 1, 2, 3$ , respectively. The minima of these plots occurs at the frequency of the eigenmode, the closer to zero the minima the higher the quality factor of the resonance. Results in each plot are shown for clusters of  $N = 4, 6, 8$ , and  $10$  particles, and it is clearly seen how the quality factor of the resonance increases with the number of scatterers. The vertical dashed line is the frequency at which the function in Eq. (18) cancels, that is to say, the frequency at which the resonance is predicted for a cluster with an infinite number of scatterers. When higher resonances are studied, some of them disappear for the smaller clusters. This is the case of  $\ell = 2$  [Fig. 2(d)], where the resonance only appears for  $N = 8$  and  $N = 10$ . Something remarkable happens in the  $\ell = 3$  case; the resonance is present in the  $N = 6$  cluster, whereas the rest of the clusters do not present any resonance. As can be seen in Fig. 4,  $\ell = 3$  shows

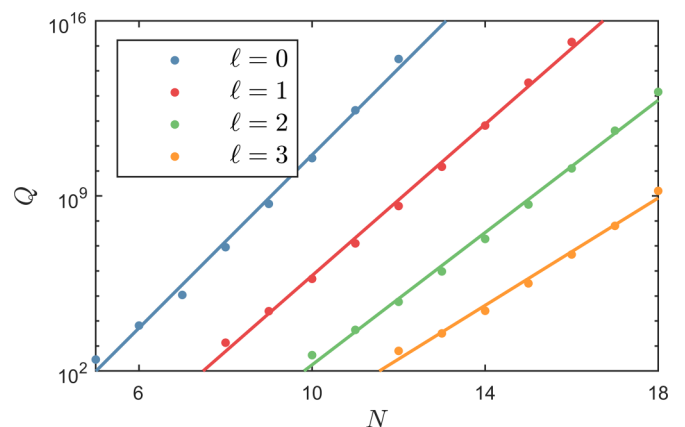


FIG. 3. Quality factor as a function of the number of scatterers in the cluster for multipolar orders  $\ell = 0, 1, 2$ , and  $3$ .

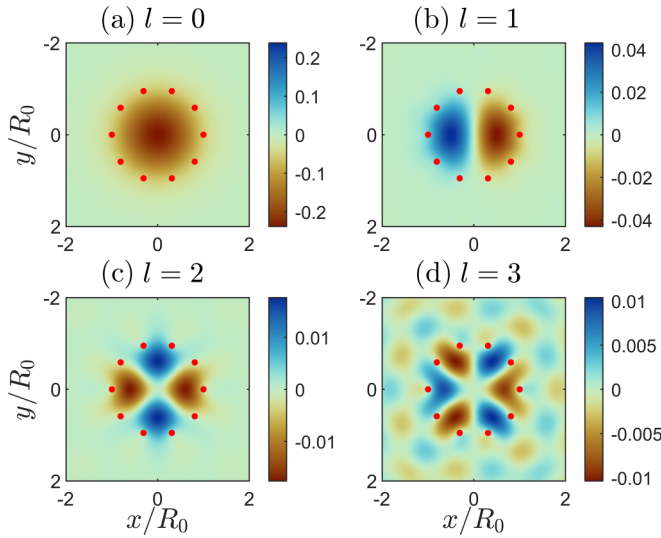


FIG. 4. Real part of the eigenfunction for different resonant index. The clusters have the same number of scatterers ( $N = 10$ ).

a  $\pi/3$  symmetry in the inner field. In fact, the resonant index  $\ell$  defines the symmetry of the eigenmode as  $\pi/\ell$ . Thus it is easier to excite this resonance when the number of scatterers is a multiple of the symmetry of the mode. When the symmetry of the cluster is different than that of the mode, the quality factor of the resonance is so small that it cannot be observed with a sweep in real frequency. It is worth mentioning that other modes appear in this analysis given that we are plotting the full multiple scattering matrix  $M$ , without any hypothesis on the symmetry of the mode, and therefore all the multipolar resonances will result in minima in the determinant of  $M$ .

The qualitative dependence of the quality factor  $Q$  of the resonance with the number of scatterers  $N$  and the multipolar order  $\ell$  can be computed as explained in Refs. [31,32], and it is shown in Fig. 3. We see that there is an exponential growth of  $Q$  with  $N$ , but we also see how  $Q$  strongly decreases with  $\ell$  for the same cluster.

Figure 4 shows the corresponding eigenfunctions for the largest cluster ( $N = 10$ ), showing how the index  $\ell$  defines the symmetry of the mode. It is also noticeable how as long as the  $\ell$  index increases, the mode is localized closer to the cluster's border; consequently, it is easier for the field to "leave" the cluster and the leakage of energy is higher than for lower  $\ell$  resonances. This is consistent with the decreasing of the quality factor of the mode with  $\ell$  shown in Fig. 3.

Modes of high index  $\ell$  tend to localize near the scatterers, resulting in the so-called whispering gallery modes. This approach allows therefore for the systematic design of high-quality whispering gallery modes. Figure 5 shows examples of these modes for a cluster of  $N = 50$  scatterers and indexes  $\ell = 5, 10, 15, 20$ . The localization of the field near the perimeter of the cluster as we increase  $\ell$  is evident in these plots.

### III. ROBUSTNESS OF THE QUASI-BIC MODES

In this section several numerical simulations are presented, the objective of which is to study how the modes get deformed

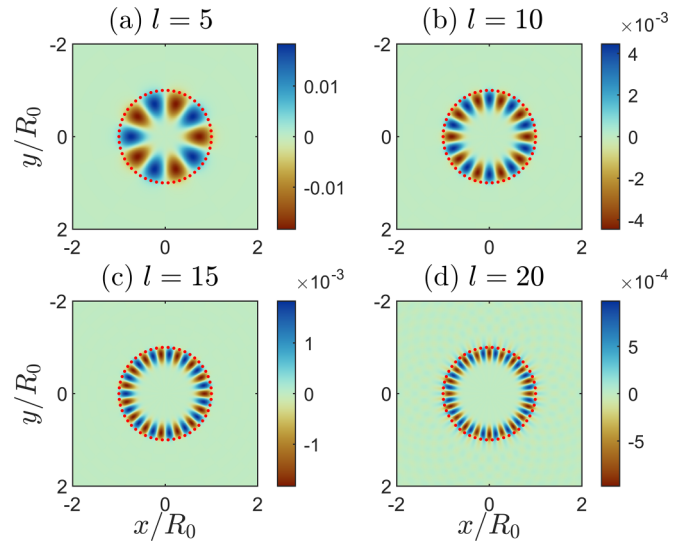


FIG. 5. Real part of the eigenfunction for different resonant index. The clusters have the same number of scatterers ( $N = 50$ ).

or destroyed when the positions of the scatterers in the cluster are perturbed.

The first situation considers missing scatterers in the polygonal arrangement. Figure 6(a) shows the plot of the minimum eigenvalue of the multiple scattering matrix as a function of frequency when all the scatterers are present (blue line), and then when we remove one (red), two (green), or three (orange) adjacent scatterers. The total number of resonators in the cluster is  $N = 20$ , and the explored resonance is  $\ell = 2$ . We see how the frequency of the resonance is slightly displaced and its quality factor decreases. The quality factor of the original resonance is  $Q = 2583$ ; remaining the same after deleting one scatterer, it gets reduced to  $Q = 736.3$  after deleting the second one and further reduced to  $Q = 60.8$  when the third resonator is removed.

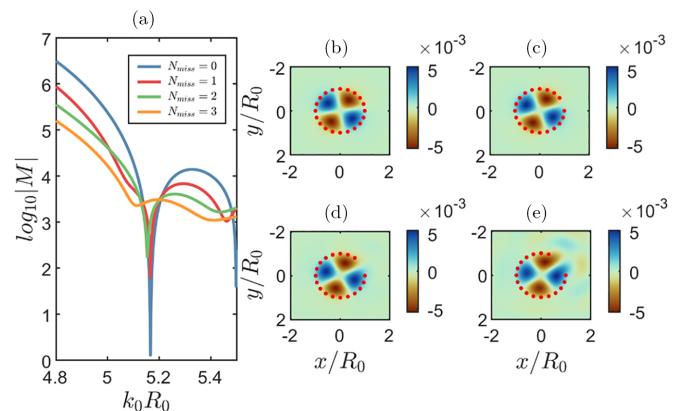


FIG. 6. Disappearance of the BIC resonance when some scatterers are missing in the circular array. At left, the evolution of the resonance; the blue line represents the cluster with all the scatterers present, in the red one one scatterer is missing, the green line is for two missing scatterers, and the orange line is for three missing scatterers. The total number of resonators is 20. The resonance index is  $\ell = 2$ . At right, both maps show the eigenfunctions (real value) for the original situation and the three-times-deformed cluster.



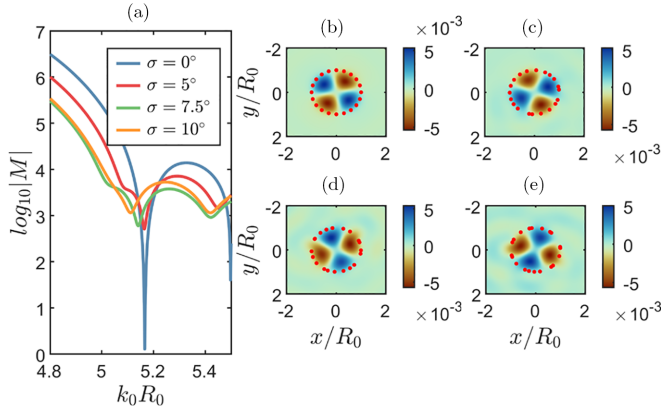


FIG. 7. Disappearance of the BIC resonance, and the position of the resonators is slightly changed. At left, the evolution of the resonance; the blue line represents the cluster at the original configuration, the red, green, and orange lines show the resonance with increasing percentage of disorder in the position of the scatterers. The maps at right show the eigenfunctions (real value) for the four configurations.

Figure 6(b)–6(e) show the maps of the mode for the different situations described above. It is clear that the symmetry of the mode is generally preserved and the field is still localized inside the cluster, although the leakage is strong when three scatterers are removed from the cluster, as can be understood from the broadening of the peak shown in panel (a).

From a practical point of view, it is also interesting to analyze the quality of the resonances with positional disorder of the particles in the cluster, since this is something we cannot avoid in practical realizations of these structures. Then the positional disorder has been applied to each scatterer in its angular position such that

$$\theta_\beta = 2\pi \frac{\beta}{N} + \sigma \mathcal{N}(0, 1), \quad (19)$$

where  $\mathcal{N}(0, 1)$  is a normal distribution of zero mean and unitary variance, and  $\sigma$  is the variance of the disorder we

aim to apply. Therefore all the scatterers remain in the same circle of radius  $R_0$ , but they are no longer equally distributed all along it.

Figure 7 shows the same results as Fig. 6 but for the positional disorder just described, with  $\sigma = 5 \times \pi/180$  for the red line,  $7.5 \times \pi/180$  for the green one, and  $10 \times \pi/180$  for the orange one. We see how the quality factor of the resonance is strongly reduced as the disorder is increased, although the quadrupolar symmetry of the mode still remains. The quality factor of the original resonance (blue line) is  $Q = 2583$ , while being  $Q = 258.2$  for the red line,  $Q = 135.3$  for the green line, and  $Q = 77.4$  for the orange one.

These results show that although the quality factor of the resonances is strongly sensitive to the perturbations of the cluster, their symmetry is a robust parameter against disorder. We have also seen that the frequency of the resonance is weakly disturbed.

#### IV. EXCITATION OF QUASI-BICS FROM THE CONTINUUM

In this section we will explore the possibility of exciting and detecting quasi-BICs by means of external incident fields to the cluster. The excitation of BICs by means of incident plane waves is impossible, since these states belong to the continuum and BICs do not couple to them. However, quasi-BICs can in principle be excited by these fields, resulting in strong peaks in the scattering cross section of the cluster, which can be used, for instance, for sensing applications.

Figure 8 shows an example of the scattered field by a cluster of  $N = 50$  scatterers when a plane wave propagates along the  $x$  axis. Simulations are shown for three different wave numbers. Panels (a) and (c) show nonresonant frequencies, while panel (b) shows the scattered field at the quasi-BIC condition, showing how, although some scattered field leaves the cluster, most of the scattering energy remains confined inside it.

The analysis of the excitation of a quasi-BIC mode can be done by means of the far-field pattern radiated by the cluster upon plane-wave incidence at frequencies near the quasi-BIC

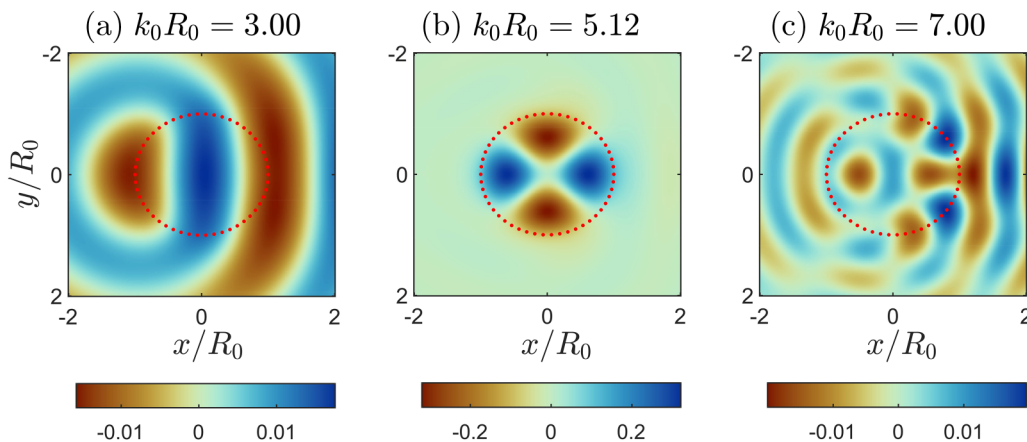


FIG. 8. Scattered field from a  $N = 50$  resonator cluster for three different frequencies. The bound state in the continuum is predicted to happen at the second frequency ( $k_0 R_0 = 5.118$ ). While the elastic field is completely located inside the circle in the middle panel, both right and left panels show the energy distributed all along the plate. The maximum displacement field is bigger in the middle panel than in the other two.

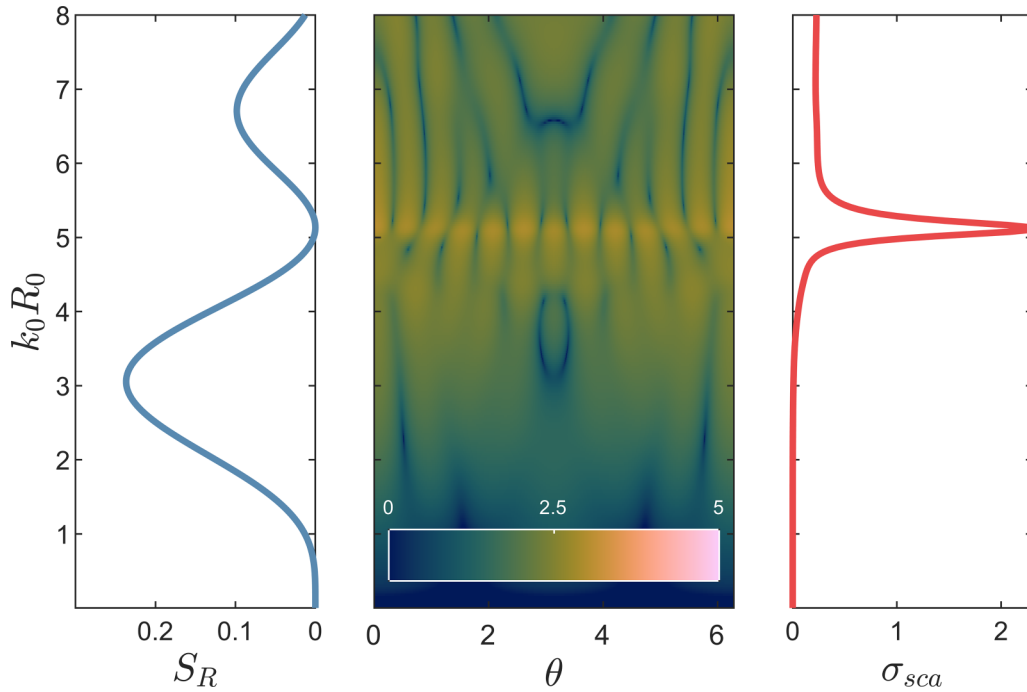


FIG. 9. Far-field radiation pattern and scattering cross section. The left graph represents the  $S_R$  term as a function of the frequency of the system. The central map shows the far-field radiation pattern  $[f(\theta)]$  as a function of the angle and the frequency. Finally, the right graph represents the scattering cross section as a function of the frequency. As it can be seen, the zero of the  $S_R$  summation term finds a peak in both the far-field radiation pattern and the scattering cross section.

condition. The far-field radiation pattern is a function of the polar angle  $\theta$  and it is given by

$$f(\theta) = \sum_{\beta=1}^N B_{\beta} e^{-ik_0 R_{\beta} \cos(\theta - \theta_{\beta})}, \quad (20)$$

and the total scattering cross section  $\sigma_{sca}$  is computed as [33]

$$\sigma_{sca} = \frac{1}{16\pi D k_0^2} \int_0^{2\pi} |f(\theta)|^2 d\theta. \quad (21)$$

Figure 9 shows the far-field analysis for the example shown in Fig. 8. The left panel shows the function  $S_R^2$ , showing the minima where the resonance is expected ( $k_0 R_0 = 5.118$ ). We can see how at this frequency there is an enhancement of the far-field pattern  $f(k_0, \theta)$  shown in the central panel, although the symmetry of this radiation pattern does not correspond to that of the quasi-BIC mode. The reason is that the mode is confined inside the cluster and thus the  $\ell = 2$  symmetry can be observed only in the near field, but this field interacts with the  $N = 50$  scatterers of the cluster and excites some far-field radiation with multipolar symmetry. The right panel shows how the total scattering cross section  $\sigma_{sca}$  is enhanced at the resonant condition, as expected.

### V. SUMMARY

In summary, we have studied the possibility of having BICs in clusters of scatterers for flexural waves in thin plates. We have found that a polygonal arrangement, which becomes a circular scatterer when the number of scatterers tends to infinite, presents resonances of a divergent quality factor; thus these modes can be defined as quasi-BIC modes. We have also

derived an analytical expression for the resonant frequency of the different multipolar resonances of the circular scatterer which is accurate as well for finite clusters. Several numerical experiments show that these modes are robust in general, in the sense that only the quality factor is significantly changed when different types of disorder are applied, while the resonant frequency is only weakly distorted. We have found as well that the quasi-BIC modes can be excited from the continuum, since a peak in the total scattering cross section is detected, which enhances the possibilities of these structures for being used in sensing applications. The formulation based on multiple scattering theory shows as well that this approach is not unique to flexural waves but could also be applied to other types of classical or quantum waves, with similar results expected.

### ACKNOWLEDGMENTS

D.T. acknowledges financial support through a ‘‘Ram3n y Cajal’’ fellowship, under Grant No. RYC-2016-21188. This research was supported by the DYNAMO project (101046489), funded by the European Union, but the views and opinions expressed are, however, those of the authors only and do not necessarily reflect those of the European Union or the European Innovation Council. Neither the European Union nor the granting authority can be held responsible for them. M.M.-S. acknowledges financial support through the FPU program under Grant No. FPU18/02725. This publication is part of Project No. PID2021-124814NB-C22, funded by MCIN/AEI/10.13039/501100011033, ‘‘FEDER, A way of making Europe.’’

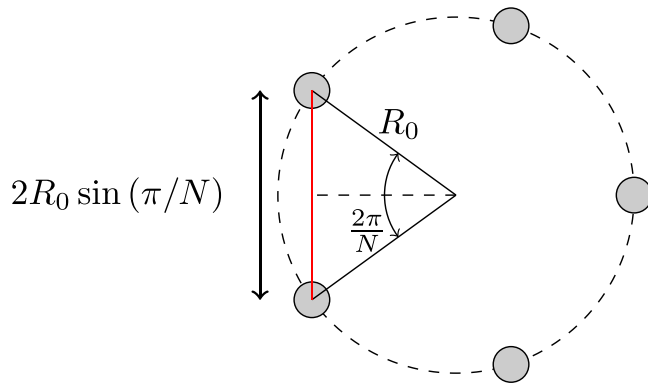


FIG. 10. Cluster geometries.

### APPENDIX: CONTINUOUS LIMIT OF THE CLUSTER'S GREEN'S FUNCTION

In this Appendix we will derive an analytical expression for the sum  $S_R^\ell$  when the number of scatterers in the circular array tends to infinite. According to Fig. 10, the scatterers in the cluster are placed in the vertices of a regular polygon of  $N$  sides, and thus the position of the  $\alpha$  scatterer is given by

$$\mathbf{R}_\alpha = R_0 \cos\left(\frac{2\pi\alpha}{N}\right)\hat{x} + R_0 \sin\left(\frac{2\pi\alpha}{N}\right)\hat{y}. \quad (\text{A1})$$

In the limit of  $N \rightarrow \infty$ , the variable  $\theta_\alpha = 2\pi\alpha/N$  can be substituted by a continuous variable  $\theta \in [0, 2\pi]$ , such that  $d\theta = 2\pi/N$ . Also, the distance  $R_{0\alpha}$  between the scatterer of reference and any scatterer in the cluster is, according to Fig. 10,

$$R_{0\alpha} = 2R_0 \sin \frac{\pi}{N}, \quad (\text{A2})$$

which, in the limit  $N \rightarrow \infty$  becomes

$$R(\theta) = 2R_0 \sin \frac{\theta}{2}. \quad (\text{A3})$$

Thus we can write

$$\lim_{N \rightarrow \infty} \frac{1}{N} S_R^\ell = \frac{1}{2\pi} \text{Re} \int_0^{2\pi} \xi(\theta) e^{i\ell\theta} d\theta, \quad (\text{A4})$$

with

$$\xi(\theta) = H_0(k_0 R(\theta)) + \frac{2i}{\pi} K_0(k_0 R(\theta)). \quad (\text{A5})$$

For  $\ell = 0$  we have

$$\begin{aligned} \lim_{N \rightarrow \infty} \frac{1}{N} S_R^0 &= \frac{1}{2\pi} \int_0^{2\pi} J_0(2k_0 R_0 \sin(\theta/2)) d\theta \\ &= \frac{2}{\pi} \int_0^{\pi/2} J_0(2k_0 R_0 \sin \theta) d\theta. \end{aligned}$$

By using the following identity [34],

$$\int_0^{\pi/2} J_{2\nu}(2z \sin x) dx = \frac{\pi}{2} J_\nu^2(z), \quad (\text{A6})$$

where  $\nu$  is the order of the Bessel function. For  $\nu = 0$  we arrive at

$$\lim_{N \rightarrow \infty} \frac{1}{N} S_R^0 = J_0^2(k_0 R_0). \quad (\text{A7})$$

Similarly, for  $\ell \neq 0$  we now have

$$\lim_{N \rightarrow \infty} \frac{1}{N} S_R^\ell = \frac{1}{2\pi} \text{Re} \int_0^{2\pi} \chi_\theta e^{i\ell\theta} d\theta. \quad (\text{A8})$$

Thus

$$\begin{aligned} &\frac{1}{2\pi} \int_0^{2\pi} J_0(2k_0 R_0 \sin \theta/2) e^{i\ell\theta} d\theta \\ &= \frac{1}{(2\pi)^2} \int_0^{2\pi} \int_{-\pi}^{\pi} e^{-i2k_0 R_0 \sin(\theta/2) \sin \tau} e^{i\ell\theta} d\tau d\theta \\ &= \frac{1}{2\pi^2} \int_0^{\pi} \int_{-\pi}^{\pi} e^{-i2k_0 R_0 \sin(\theta) \sin \tau} e^{2i\ell\theta} d\tau d\theta \\ &= \frac{(-1)^{2\ell}}{2\pi} \int_{-\pi}^{\pi} J_{2\ell}(2k_0 R_0 \sin \tau) d\tau \\ &= \frac{2(-1)^{2\ell}}{\pi} \int_0^{\pi/2} J_{2\ell}(2k_0 R_0 \sin \tau) d\tau \end{aligned}$$

so that we have

$$\lim_{N \rightarrow \infty} \frac{1}{N} S_R^\ell = J_\ell^2(k_0 R). \quad (\text{A9})$$

- [1] J. v. Neumann and E. P. Wigner, Über merkwürdige diskrete eigenwerte, *Phys. Z.* **30**, 465 (1929).  
 [2] I. Quotane, E. H. El Boudouti, and B. Djafari-Rouhani, Trapped-mode-induced fano resonance and acoustical transparency in a one-dimensional solid-fluid phononic crystal, *Phys. Rev. B* **97**, 024304 (2018).  
 [3] Y. Jin, E. H. E. Boudouti, Y. Pennec, and B. Djafari-Rouhani, Tunable fano resonances of Lamb modes in a pillared metasurface, *J. Phys. D* **50**, 425304 (2017).

- [4] S. Mizuno, Fano resonances and bound states in the continuum in a simple phononic system, *Appl. Phys. Express* **12**, 035504 (2019).  
 [5] M. Amrani, I. Quotane, C. Ghouila-Houri, E. H. El Boudouti, L. Krutyanskiy, B. Piwakowski, P. Pernod, A. Talbi, and B. Djafari-Rouhani, Experimental Evidence of the Existence of Bound States in the Continuum and Fano Resonances in Solid-Liquid Layered Media, *Phys. Rev. Appl.* **15**, 054046 (2021).



- [6] L. Huang, B. Jia, A. S. Pilipchuk, Y. Chiang, S. Huang, J. Li, C. Shen, E. N. Bulgakov, F. Deng, D. A. Powell *et al.*, A general framework of bound states in the continuum in an open acoustic resonator, *Phys. Rev. Applied* **18**, 054021 (2022).
- [7] T. Mrabti, Z. Labdouti, A. Mouadili, E. El Boudouti, and B. Djafari-Rouhani, Aharonov-Bohm-effect induced transparency and reflection in mesoscopic rings side coupled to a quantum wire, *Phys. E* **116**, 113770 (2020).
- [8] T. Mrabti, Z. Labdouti, O. El Abouti, E. El Boudouti, F. Fethi, and B. Djafari-Rouhani, Transmission gaps, trapped modes and fano resonances in Aharonov–Bohm connected mesoscopic loops, *Phys. Lett. A* **382**, 613 (2018).
- [9] C. W. Hsu, B. Zhen, S.-L. Chua, S. G. Johnson, J. D. Joannopoulos, and M. Soljačić, Bloch surface eigenstates within the radiation continuum, *Light Sci. Appl.* **2**, e84 (2013).
- [10] A. F. Sadreev, Interference traps waves in an open system: Bound states in the continuum, *Rep. Prog. Phys.* **84**, 055901 (2021).
- [11] E. N. Bulgakov and A. F. Sadreev, Bound states in the continuum in photonic waveguides inspired by defects, *Phys. Rev. B* **78**, 075105 (2008).
- [12] F. Wu, J. Wu, Z. Guo, H. Jiang, Y. Sun, Y. Li, J. Ren, and H. Chen, Giant Enhancement of the Goos-Hänchen Shift Assisted by Quasibound States in the Continuum, *Phys. Rev. Appl.* **12**, 014028 (2019).
- [13] F. Yesilkoy, E. R. Arvelo, Y. Jahani, M. Liu, A. Tittl, V. Cevher, Y. Kivshar, and H. Altug, Ultrasensitive hyperspectral imaging and biodetection enabled by dielectric metasurfaces, *Nat. Photonics* **13**, 390 (2019).
- [14] L. Kühner, L. Sortino, R. Berté, J. Wang, H. Ren, S. A. Maier, Y. Kivshar, and A. Tittl, Radial bound states in the continuum for polarization-invariant nanophotonics, *Nat. Commun.* **13**, 4992 (2022).
- [15] A. Taghizadeh, J. Mørk, and I.-S. Chung, Ultracompact resonator with high quality-factor based on a hybrid grating structure, *Opt. Express* **23**, 14913 (2015).
- [16] H. Zhang, T. Wang, J. Tian, J. Sun, S. Li, I. De Leon, R. P. Zaccaria, L. Peng, F. Gao, X. Lin *et al.*, Quasi-BIC laser enabled by high-contrast grating resonator for gas detection, *Nanophotonics* **11**, 297 (2022).
- [17] G. Yadav, S. Sahu, R. Kumar, and R. Jha, Bound states in the continuum empower subwavelength gratings for refractometers in visible, *Photonics* **9**, 292 (2022).
- [18] A. L. Krishna, S. Menon, A. Prosad, and V. Raghunathan, Mid-infrared quasi-BIC resonances with sub-wavelength slot mode profiles in germanium-based coupled guided-mode resonance structures, *Photon. Res.* **10**, 68 (2022).
- [19] F. Wu, M. Luo, J. Wu, C. Fan, X. Qi, Y. Jian, D. Liu, S. Xiao, G. Chen, H. Jiang *et al.*, Dual quasibound states in the continuum in compound grating waveguide structures for large positive and negative Goos-Hänchen shifts with perfect reflection, *Phys. Rev. A* **104**, 023518 (2021).
- [20] I. V. Timofeev, D. N. Maksimov, and A. F. Sadreev, Optical defect mode with tunable q factor in a one-dimensional anisotropic photonic crystal, *Phys. Rev. B* **97**, 024306 (2018).
- [21] J. Jin, X. Yin, L. Ni, M. Soljačić, B. Zhen, and C. Peng, Topologically enabled ultrahigh-q guided resonances robust to out-of-plane scattering, *Nature (London)* **574**, 501 (2019).
- [22] Z. Zhang, J. Yang, T. Du, H. Ma, and X. Jiang, Tailoring bound states in the continuum in symmetric photonic crystal slabs by coupling strengths, *Opt. Express* **30**, 8049 (2022).
- [23] S. Liu, H. Tong, and K. Fang, Optomechanical crystal with bound states in the continuum, *Nat. Commun.* **13**, 3187 (2022).
- [24] A. Taghizadeh and I.-S. Chung, Quasi bound states in the continuum with few unit cells of photonic crystal slab, *Appl. Phys. Lett.* **111**, 031114 (2017).
- [25] L. Huang, W. Zhang, and X. Zhang, Moiré Quasibound States in the Continuum, *Phys. Rev. Lett.* **128**, 253901 (2022).
- [26] C. W. Hsu, B. Zhen, A. D. Stone, J. D. Joannopoulos, and M. Soljačić, Bound states in the continuum, *Nat. Rev. Mater.* **1**, 16048 (2016).
- [27] H. Putley, G. Chaplain, H. Rakotoarimanga-Andrianjaka, B. Maling, and R. Craster, Whispering-Bloch elastic circuits, *Wave Motion* **105**, 102755 (2021).
- [28] D. Torrent, D. Mayou, and J. Sánchez-Dehesa, Elastic analog of graphene: Dirac cones and edge states for flexural waves in thin plates, *Phys. Rev. B* **87**, 115143 (2013).
- [29] P. Packo, A. N. Norris, and D. Torrent, Inverse Grating Problem: Efficient Design of Anomalous Flexural Wave Reflectors and Refractors, *Phys. Rev. Appl.* **11**, 014023 (2019).
- [30] M. Martí-Sabaté and D. Torrent, Dipolar Localization of Waves in Twisted Phononic Crystal Plates, *Phys. Rev. Appl.* **15**, L011001 (2021).
- [31] M. Martí-Sabaté and D. Torrent, Edge modes for flexural waves in quasi-periodic linear arrays of scatterers, *APL Mater.* **9**, 081107 (2021).
- [32] M. Martí-Sabaté, S. Guenneau, and D. Torrent, High-quality resonances in quasi-periodic clusters of scatterers for flexural waves, *AIP Adv.* **12**, 085303 (2022).
- [33] P. Packo, A. N. Norris, and D. Torrent, Metaclusters for the Full Control of Mechanical Waves, *Phys. Rev. Appl.* **15**, 014051 (2021).
- [34] I. S. Gradshteyn and I. M. Ryzhik, *Table of Integrals, Series, and Products* (Academic Press, New York, 2014).